

Anisotropic damping of the magnetization dynamics in Ni, Co, and Fe

Keith Gilmore and M. D. Stiles

National Institute of Standards and Technology, Center for Nanoscale Science and Technology, Gaithersburg, Maryland 20899-6202, USA

Jonas Seib, Daniel Steiauf, and Manfred Fähnle*

Max-Planck-Institut für Metallforschung, Heisenbergstraße 3, 70569 Stuttgart, Germany

(Received 25 September 2009; revised manuscript received 8 March 2010; published 17 May 2010)

The Gilbert parameter α describing the damping of magnetization dynamics is commonly taken to be an isotropic scalar. We argue that it is a tensor $\underline{\alpha}$ that is anisotropic, leading to a dependence of the damping on both the instantaneous direction of the magnetization $\mathbf{M}(t)$ (orientational anisotropy) and on the direction of rotation of the magnetization (rotational anisotropy). For small-angle precession of \mathbf{M} around a prescribed axis in the crystal, the rotational anisotropy of Ni, Co, and Fe is calculated as a function of the electronic scattering rate. For circular precession, the rotational anisotropy of \mathbf{M} is averaged out and the damping is determined by an effective damping scalar α_{eff} which depends on the axis of rotation. The quantity α_{eff} of Ni, Co, and Fe is calculated for various crystallographic orientations. All calculations are performed by the *ab initio* density-functional electron theory within the framework of the torque-correlation model. The intraband contribution of this model (breathing Fermi-surface contribution) maintains both orientational and rotational anisotropy for all scattering rates. In contrast, the interband contribution (bubbling Fermi-surface contribution) exhibits these anisotropies only at small scattering rates (τ^{-1}) and becomes increasingly isotropic (both orientationally and rotationally) as τ^{-1} increases. Because the interband contribution dominates at high τ^{-1} , each material should exhibit isotropic damping at sufficiently high τ^{-1} (i.e., sufficiently high temperatures).

DOI: [10.1103/PhysRevB.81.174414](https://doi.org/10.1103/PhysRevB.81.174414)

PACS number(s): 75.40.Gb, 76.60.Es, 76.50.+g

I. INTRODUCTION

In recent years there has been a steadily growing interest in fast magnetization dynamics on time scales between several picoseconds and nanoseconds, especially for micro-sized and nano-sized magnets because of their potential use in advanced information storage and data processing devices. Examples are the dynamics of domain walls in nanowires,¹ the magnetization reversal in nanomagnets,¹ and the dynamics of vortices.² From a theoretical point of view, most investigations have been simulations based on Gilbert's equation of motion³ for the magnetization $\mathbf{M}(\mathbf{r}, t)$,

$$\frac{d\mathbf{M}}{dt} = -\gamma(\mathbf{M} \times \mathbf{H}_{\text{eff}}) + \frac{1}{M}\mathbf{M} \times \alpha \frac{d\mathbf{M}}{dt}, \quad (1)$$

or on extensions of this equation including the effect of spin-polarized transport currents. In Eq. (1) the first term describes the precession around an effective field \mathbf{H}_{eff} (γ is the gyromagnetic ratio). The second term describes the damping, i.e., the relaxation of the magnetization direction toward the equilibrium orientation parallel to \mathbf{H}_{eff} , and α is the damping parameter which is typically treated as a scalar constant.

More recently, various theoretical approaches have suggested that for a more realistic description of the magnetization dynamics Gilbert's damping term should be replaced by a more complicated form. For instance, the damping scalar α has been replaced⁴⁻¹² by a damping matrix $\underline{\alpha}$. This represents a first type of anisotropy of the damping, because it means that the damping is different for different directions of the change $d\mathbf{M}/dt$ of the magnetization (rotational anisotropy). Furthermore, it has been proposed^{5,7-11} that $\underline{\alpha}$ depends on the momentary configuration $\mathbf{M}(\mathbf{r}, t)$. For the case of a collinear

system, e.g., this represents a second type of anisotropy (orientational anisotropy) because the damping depends on the momentary orientation of $\mathbf{M}(t)$. Finally, it has been noted^{6,8} that in general, e.g., for a noncollinear configuration $\mathbf{M}(\mathbf{r}, t)$, the damping matrix is nonlocal, i.e., it relates the time derivative $d\mathbf{M}(\mathbf{r}, t)/dt$ at site \mathbf{r} to the derivatives $d\mathbf{M}(\mathbf{r}', t)/dt$ at other sites \mathbf{r}' .

The rotational anisotropy arises from the fact that the damping matrix has two nonzero eigenvalues which are unequal for an arbitrary orientation of the magnetization with respect to the crystal axes. The orientational anisotropy occurs because both eigenvalues depend on the magnetization direction. For a magnetization direction which corresponds to a threefold or fourfold symmetry direction of the crystal the two eigenvalues are the same, i.e., there is no rotational anisotropy. In a ferromagnetic resonance experiment, the strong external dc field selects a crystal orientation about which the magnetization vector precesses under the action of an additional small perpendicular ac field. If the field is strong enough that the precession is circular, it has been shown¹¹ that the rotational anisotropy is averaged out: the FMR linewidth is to a very good approximation described by an effective damping scalar α_{eff} which is just the arithmetic mean of the two eigenvalues for the magnetization direction prescribed by the dc field. Because of the orientational anisotropy of the two eigenvalues, α_{eff} depends on the orientation of the dc field.

In the present paper we consider the temperature dependence of both the rotational and the orientational anisotropy. The anisotropy and its temperature dependence will be different for different physical processes leading to damping (a review on different damping mechanisms is given in Ref. 13). We confine ourselves to the damping due to the creation

of electron-hole pairs resulting from time-dependent spin-orbit interactions and their subsequent relaxation via scattering at phonons or lattice defects. This process is the dominant damping mechanism in metallic ferromagnets. The theoretical approaches to describe this mechanism may be subdivided into two categories: in the first category the damping parameter is determined from the low-frequency limit of the transverse-spin-response function which is calculated using model Hamiltonians^{14,15} or time-dependent spin-density-functional electron theory.¹⁶ In the second category^{7,8,17,18} an effective field for the magnetization dynamics is defined as the variation in the electronic energy with respect to the magnetization direction, $\delta E / \delta \mathbf{M}$. In a static situation this effective field is equivalent to the magnetocrystalline anisotropy field, whereas in a dynamical situation irreversible contributions appear which give rise to damping. The relation between these two approaches is discussed in Refs. 18 and 19. It is common to all these approaches that the creation of electron-hole pairs is treated explicitly, whereas the subsequent relaxation due to scattering at phonons or defects is accounted for just phenomenologically by a finite lifetime τ of the states entering the electron spectral functions^{15,16,18–20} or by a relaxation time for the nonequilibrium occupation numbers for the electronic states.

The above-mentioned theories have shown that the contributions to the damping originating from the creation of electron-hole pairs can be divided into two terms, one that decreases with temperature like the electrical conductivity does and one that increases with temperature like the resistivity does. In the case of Ni these two contributions have been resolved very clearly in experiments.²¹ For the conductivitylike contribution a generalized Gilbert equation could be derived (see above) from an effective field approach^{7,8} for a general trajectory of $\mathbf{M}(t)$ in which the constant Gilbert scalar α is replaced by a matrix $\underline{\alpha}[\mathbf{M}(t)]$ so that both the rotational and orientational damping anisotropies are included. The calculations for the resistivitylike contribution^{14–16,18,20,22} consider the reaction of the system for a special trajectory of $\mathbf{M}(t)$. For the small-angle circular precession of $\mathbf{M}(t)$ around a prescribed direction, like in a FMR experiment, the resistivitylike terms yield the effective damping scalar α_{eff} for that prescribed direction. The rotational anisotropy of this contribution may be found from considering elliptical trajectories of $\mathbf{M}(t)$ about the prescribed direction. In the present paper both the conductivitylike and the resistivitylike contributions to the rotational and orientational anisotropies are calculated. The purpose of this work is to compare the anisotropies of these two contributions as functions of the scattering rate of the electrons in order to quantify the validity of neglecting this effect in the analysis of experimental results.

II. DAMPING DUE TO THE CREATION OF ELECTRON-HOLE PAIRS

In some of the formal derivations of the equations for damping the physics underlying the conductivitylike and the resistivitylike contributions is hard to recognize. Therefore,

the two contributions have been illuminated more clearly by rederiving them from approaches which are designed in such a way that the underlying physics becomes more apparent.^{18,19} Before presenting the numerical calculations of the anisotropic damping, we want to approach the two contributions from a further and alternative viewpoint, hoping that this leads to an even more improved understanding of the physics of damping. Both contributions are related to the generation of electron-hole pairs by the magnetization dynamics. The subsequent relaxation of the excited electrons and the holes by scattering at phonons or lattice defects in general will transfer angular momentum from the spin system to the lattice, and this is responsible for the damping of the magnetization dynamics. We focus on the physics behind the generation of the electron-hole pairs; the scattering is accounted for phenomenologically via a relaxation time τ .

In the following we consider a situation for which the micromagnetic magnetization entering Eq. (1) is homogeneous, i.e., $\mathbf{M}(\mathbf{r}, t) = \mathbf{M}(t) = M\mathbf{e}(t)$. [$\mathbf{e}(t)$ is a unit vector in the magnetization direction.] Furthermore, we are only interested in the temporal evolution of the system on the time scale of ns to several ps. Then $\mathbf{M}(t)$ may be obtained from the microscopic spin magnetization density $\mathbf{m}(\mathbf{r}, t)$ by a coarse-graining procedure,²³

$$\mathbf{M}(t) = M\mathbf{e}(t) = \frac{1}{\Omega} \frac{\nu}{2} \int_{\Omega} d^3r \int_{t-1/\nu}^{t+1/\nu} dt' \mathbf{m}(\mathbf{r}, t'), \quad (2)$$

where Ω is the volume of the sample and where the integration in time averages over the fast magnetic degrees of freedom, i.e., over the fluctuations on a time scale shorter than the inverse of the frequency ν of a typical long-wavelength spin wave.

For a complete quantum mechanical description of magnetization dissipation, i.e., of the transfer of angular momentum and energy from the electronic system to the lattice, one must start from the time-dependent wave equation for electrons and nuclei, involving spin-orbit coupling which mediates this transfer. Instead, we will describe the situation by an effective single-electron theory that involves only electrons and holes and that describes the energy and momentum transfer as a scattering of electrons or holes with the lattice, which is accounted for phenomenologically by the aforementioned lifetime (relaxation time) τ .

The single electron states we use are the Kohn-Sham eigenstates of density-functional theory. Density-functional theory allows for a formally rigorous calculation of the ground state energy and density of an interacting electronic system. In the Kohn-Sham approach, the density is constructed from an effective single electron theory. The eigenvalues and eigenvectors of this calculation form a simple and accurate single electron approximation for the electronic structure of many solids including transition metals.

We want to approach the problem from two opposing limits, i.e., $\tau \rightarrow 0$ and $\tau \rightarrow \infty$. In the first case the electronic scattering processes are so frequent that the electronic system is always in its ground state (“equilibrium”) with respect to the momentary orientation $\mathbf{e}(t)$ which can be considered as an external parameter. Then we can define [e.g., by the solution

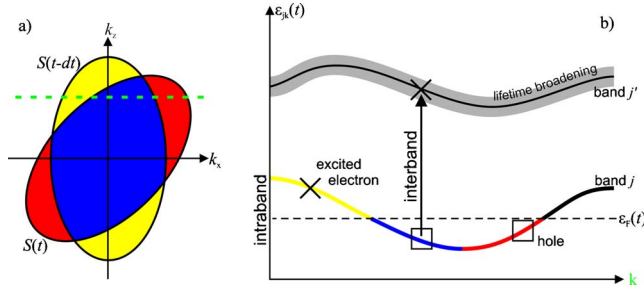


FIG. 1. (Color online) A sketch of the equilibrium Fermi surface S for time $t-dt$ and time t [(a), left part]. In a strict equilibrium situation the yellow (light gray) states are occupied only at time $t-dt$, the red (gray) states are occupied only at time t , whereas the blue (dark gray) states are occupied at both times. Panel (b) (right part) shows a sketch of the equilibrium band structure $\varepsilon_{jk}(t)$ along the direction in k space indicated by the horizontal dashed line in (a). For a realistic situation where the n_{jk} lag behind the f_{jk} there may be some yellow (light gray) states which should be empty in a strict equilibrium situation but which are occupied in a realistic situation. Furthermore, there may be some red (gray) states which should be occupied but which are still empty. In (b) there is also a sketch for the interband transitions.

of the Kohn-Sham equations of the density-functional electron theory for prescribed $\mathbf{e}(t)$] equilibrium single-electron energies $\varepsilon_{jk}(\mathbf{e}(t))$, where j and \mathbf{k} denote the band index and the wave vector, the corresponding wave functions $|\psi_{jk}(\mathbf{e}(t))\rangle$, the equilibrium Fermi-Dirac occupation numbers $f_{jk}(\mathbf{e}(t))$ and the equilibrium Fermi surface $S(\mathbf{e}(t))$. Because of the action of the spin-orbit coupling, all these quantities change in time when \mathbf{e} changes in time, i.e., the Fermi surface will continuously attain a slightly different form [breathing Fermi surface Fig. 1(a)]. It can be shown by quantum mechanical arguments²³ that in the equilibrium situation there is no damping at all.

For the opposing case, $\tau \rightarrow \infty$, there are no scattering processes at all and hence again no damping. The many-electron wave function $\Psi(t)$ for the N electrons then evolves in time coherently according to the time-dependent Schrödinger equation. As initial condition $\Psi(t=0)$ we can use, e.g., the equilibrium many-electron wave function for an initial orientation $\mathbf{e}(t=0)$ which does not correspond to a high-symmetry direction of the crystal. From $\Psi(t)$ we can calculate the microscopic spin-magnetization $\mathbf{m}(\mathbf{r}, t)$, from which the momentary $\mathbf{e}(t)$ are obtained by use of Eq. (2). From the solution of the Kohn-Sham equations for this $\mathbf{e}(t)$ the equilibrium quantities $\varepsilon_{jk}(\mathbf{e}(t))$, $\psi_{jk}(\mathbf{e}(t))$, $f_{jk}(\mathbf{e}(t))$, and $S(\mathbf{e}(t))$ are determined. Finally, we can represent the many electron wave function $\Psi(t)$ by the equilibrium single-electron wave functions $\psi_{jk}(\mathbf{e}(t))$. The occupation numbers $n_{jk}(t) = \langle \Psi(t) | \hat{a}_{kj}^\dagger \hat{a}_{kj} | \Psi(t) \rangle$, where $\hat{a}_{kj}^\dagger, \hat{a}_{kj}$ is the particle number operator for the single-electron state (jk) , in general will be different from the equilibrium occupation numbers $f_{jk}(\mathbf{e}(t))$. This occurs because without scattering the electronic system will be driven away from the equilibrium situation, i.e., there will be a generation of excited electrons and holes when we consider the equilibrium situation as the corresponding momentary reference situation.

In a realistic situation there are scattering processes which require a finite time (i.e., τ is nonzero and finite) and which

tend to drive the occupation numbers $n_{jk}(t)$ toward the equilibrium occupation numbers $f_{jk}(t)$ by a relaxation of the electron-hole pairs. We can distinguish between pairs for which the electrons and holes appear in the same equilibrium band, respectively, and pairs for which electrons and holes are generated by transitions between different bands. To illustrate the physical reason for the generation of these two types of pairs it is convenient to consider the situation from the viewpoint of the hypothetical equilibrium reference situation. The intraband pairs are generated because the spin-orbit energy of each equilibrium single electron state changes when $\mathbf{e}(t)$ varies in time. Some states which were just below the Fermi surface for time $t-dt$ get pushed above the Fermi surface for time t , whereas other states which were originally above are pushed below. For very frequent scattering processes the real many-electron wave function would evolve according to $n_{jk}(t) = f_{jk}(t)$, and there would be no damping at all (see above). For finite τ , however, the actual occupation numbers $n_{jk}(t)$ lag behind the equilibrium occupation numbers $f_{jk}(t)$. Therefore it may be that at time t some of the equilibrium states which were originally occupied at time $t-dt$ and which would be empty in an equilibrium situation are still occupied, whereas some other states which should be occupied are still empty [Fig. 1(b)]. The intraband relaxation of these electron-hole pairs leads to the transfer of angular momentum from the spin system to the lattice. This so-called intraband or *breathing Fermi-surface contribution*^{7,8,17-20} to damping increases linearly with τ and thus represents the conductivitylike term.

The interband pairs are generated because the system of equilibrium single-electron wave functions ψ_{jk} feels a time-dependent perturbation due to the changing spin-orbit interaction, and this leads to band transitions between the equilibrium states $\psi_{jk}(\mathbf{e}(t))$ and $\psi_{j'k}(\mathbf{e}(t))$. [The initial and final states have the same wave vector \mathbf{k} because the transitions are caused by the uniform mode $\mathbf{e}(t)$ which has a wave vector of zero.] Thereby, the number of final states accessible by the perturbation increases with decreasing τ due to the lifetime broadening of the states [Fig. 1(b)], and it turns out that this so-called¹⁸ interband or *bubbling Fermi-surface contribution* to damping increases monotonically with $1/\tau$ and hence represents the resistivitylike term. It has been shown in Refs. 18 and 19 that the breathing and the bubbling Fermi-surface contributions obtained from the physical reasoning of this and the previous paragraph are identical to the intraband and interband contributions of Kamberský's torque correlation model.¹⁵

The phenomenological use of a single lifetime to describe electron scattering is not without its drawbacks. Previous authors¹⁶ have shown that while this approximation works well in the long lifetime limit, i.e., for the intraband terms discussed below, vertex corrections can be important in the short lifetime limit. How important these corrections are depends on the system, both its electronic structure and the explicit mechanism behind the lifetime. Such calculations are becoming feasible for specific realizations of disorder for model calculations¹⁶ and for large scale electronic structure calculations⁹ when the disorder responsible for the electron lifetime is known. In the case of interest here, in which we are studying the temperature dependence of the damping in

nominally pure metals, it is phonons that are responsible for the electron scattering. Improving on our phenomenological lifetime τ will require the rather computational intensive approach of explicit calculation of the electron-phonon scattering rates. Such a calculation is probably not feasible at the present and likely only to change our results quantitatively, not qualitatively.

III. RESULTS

We calculate the damping rate for Ni, Co, and Fe from a generalization of Kambersky's torque correlation model. In deriving his model, Kambersky makes approximations based on the assumption that the small angle precession is both circular and around a high-symmetry direction. However, these restrictions are not necessary; we generalize the derivation of Garate and MacDonald¹⁶ for precessional motion of arbitrary ellipticity. In parallel, we linearize the Gilbert equation with the damping matrix. Comparing the two results the damping matrix can be extracted. Furthermore, we determined the effective damping rate for an arbitrary elliptical trajectory that corresponds to the energy relaxation rate averaged over a period. To illustrate the orientational anisotropy, we compute the effective damping for circular precession, then to illustrate the rotational anisotropy we compute the effective damping for precession of varying ellipticity around a few lower symmetry points. While it is likely impossible to measure "linear" precession experimentally, it is possible theoretically to set up such a case and directly extract the damping matrix. These results agree well with earlier results for the conductivitylike contribution.⁸

Figure 2 shows results for Ni, Co, and Fe for the rotationally averaged effective damping constant α_{eff} for circular precession as a function of the inverse lifetime τ^{-1} for various directions of the prescribed axis around which the magnetization vector precesses. As discussed in Sec. I, for the high-symmetry directions (which are $\langle 001 \rangle$ and $\langle 111 \rangle$ in Ni and Fe and $\langle 0001 \rangle$ in Co) the two eigenvalues of the damping matrix are the same and thus α_{eff} is identical to that eigenvalue. We present the total, intraband, and interband contributions of Kambersky's torque correlation model as calculated by the linear augmented plane wave (LAPW) method in the local spin-density approximation. In the LAPW approximation, the electronic states are described by atomiclike wave functions near the atomic cores and by plane waves in the interstitial region between them. This approach provides a very accurate description of the Kohn-Sham eigenstates near the atomic cores where spin-orbit coupling is important. Details of the calculation are given in Refs. 19 and 24.

It becomes obvious from Fig. 2 that for small τ^{-1} the conductivitylike contribution dominates whereas for increasing temperature the resistivitylike contribution takes over so that the damping exhibits a minimum. Whatever the relation $\tau(T)$, the calculated minimum can be compared directly and quantitatively with the experimentally measured minimum. It has been shown in Ref. 19 that for Ni $\langle 111 \rangle$ and Fe $\langle 001 \rangle$ these two values agree rather well, demonstrating that the torque correlation model accounts for the dominant contribu-

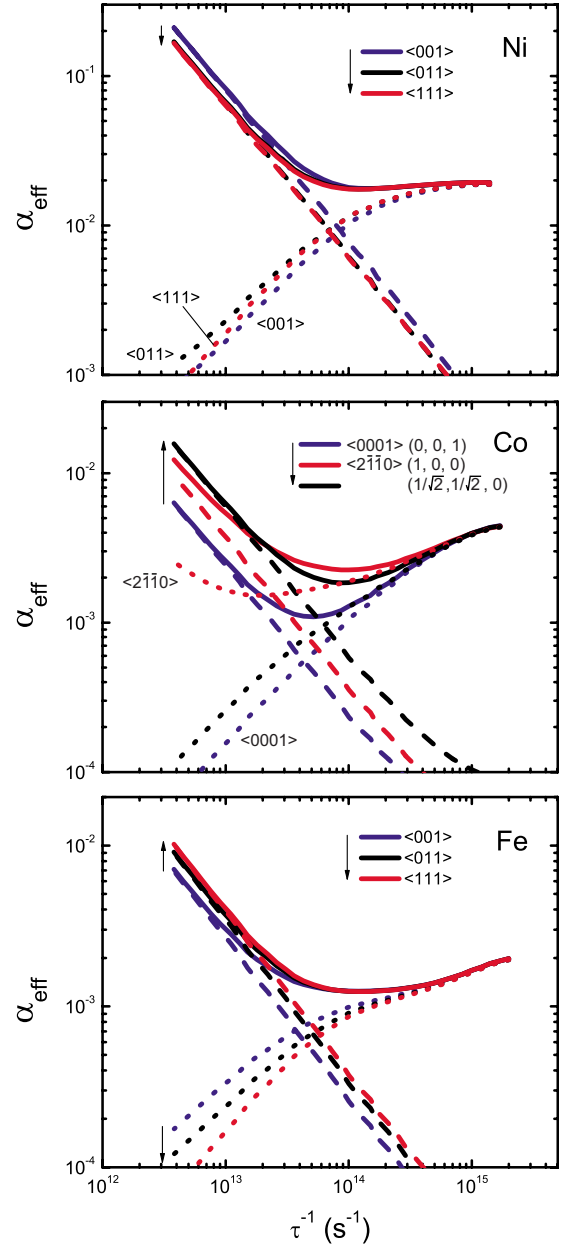


FIG. 2. (Color online) The effective damping parameter α_{eff} for circular precession for Ni (top), Co (middle), and Fe (bottom) vs electron scattering rate τ^{-1} , for various orientations of the prescribed axis around which the small-angle precession of the magnetization vector takes place. The convention for the real-space coordinate directions for Co are described in the text. Full lines: total damping, dashed lines: conductivitylike contribution and dotted lines: resistivitylike contribution.

tion to damping in these systems. One present objective is to compare the orientational anisotropy of α_{eff} of the intraband and interband contributions. Since the electron scattering rate τ^{-1} increases with the number of thermally excited phonons, the results give a qualitative sense for the temperature dependence of the anisotropy of the damping.

Calculations of α_{eff} were performed for a number of orientations; but for the purposes of clarity results for only a few of these orientations are presented in Fig. 2. The present

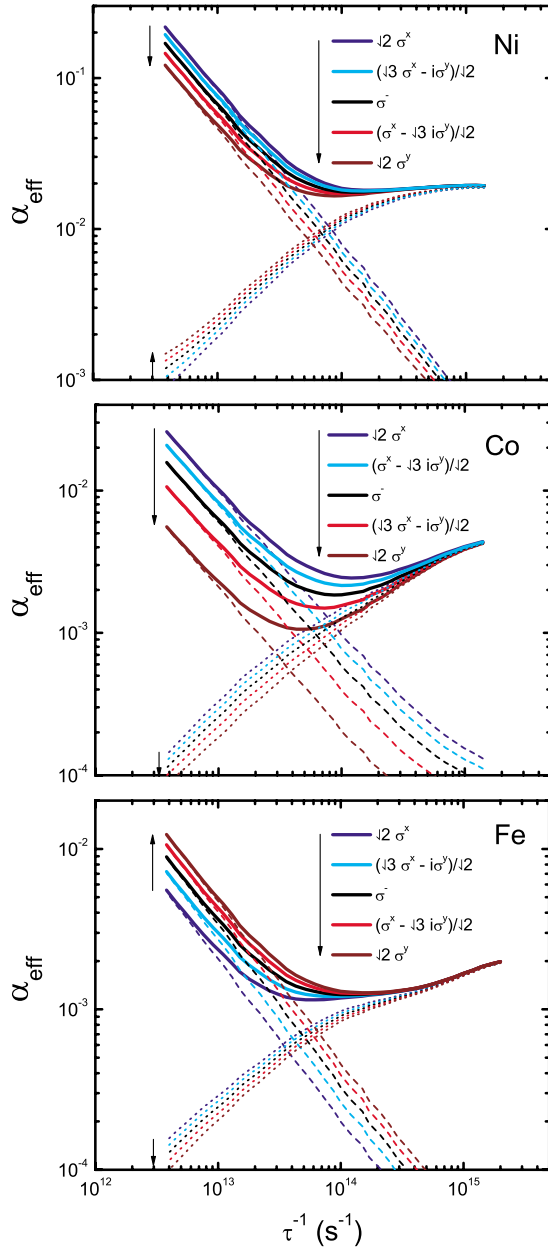


FIG. 3. (Color online) The effective damping parameter α_{eff} for Ni (top), Co (middle), and Fe (bottom) vs electron scattering rate τ^{-1} for various ellipticities of orbit about the prescribed axis, which is $\langle 011 \rangle$ for Ni and Fe, and the real-space $(1, 0, 1)/\sqrt{2}$ direction for Co. Ellipticities and real-space axes convention are as described in the text. Full lines: total damping, dashed lines: conductivitylike contribution and dotted lines: resistivitylike contribution.

findings corroborate previous work⁸ that investigated the orientational anisotropy of the eigenvalues of the conductivitylike contribution to the damping parameter. We find here that the orientational anisotropy present in these eigenvalues is maintained in the conductivitylike contribution of the rotationally averaged α_{eff} and that this anisotropy persists for all τ^{-1} . The conductivitylike contribution to α_{eff} for all directions tested in Ni and Fe was bounded by the values for the high-symmetry directions, while for Co the high-symmetry direction yielded the minimal α_{eff} of all orientations tested.

While the conductivitylike contribution is anisotropic for all τ^{-1} , the anisotropy of the resistivitylike contribution decreases with increasing τ^{-1} (i.e., with increasing temperature). Anisotropy of the resistivitylike contribution arises when the number of interband transitions that occur for a given lifetime broadening of the states is different for the band structure belonging to one orientation than for the band structure belonging to another orientation. When the lifetime broadening is much larger than the energy differences that occur when switching between orientations, then equally many transitions are allowed for the different orientations, i.e., the damping becomes isotropic. For the resistivitylike contribution, as $\hbar\tau^{-1}$ becomes comparable to the d -band width at very high scattering rates α_{eff} varies only slightly with the scattering rate and the result saturates. (Note, however, that for the case of extremely high scattering rates our theory no longer applies.)

Whether intrinsic damping is orientationally isotropic at room temperature depends on the details of the band structure and the strength of the spin-orbit coupling of the material under consideration. For Ni, both the conductivitylike and the resistivitylike contributions could be resolved experimentally,²¹ with a dominance of the conductivitylike term at least up to room temperature. An anisotropy of the FMR linewidth has been found for Ni in Ref. 25 in which the linewidth increased according to $(\Delta H)_{\langle 001 \rangle} < (\Delta H)_{\langle 111 \rangle} < (\Delta H)_{\langle 011 \rangle}$ at $T=4$ K and $(\Delta H)_{\langle 111 \rangle} < (\Delta H)_{\langle 001 \rangle} < (\Delta H)_{\langle 011 \rangle}$ at $T=77$ K. In our calculations we found for the conductivitylike contribution $\alpha_{\langle 111 \rangle} < \alpha_{\langle 011 \rangle} < \alpha_{\langle 001 \rangle}$. One possible reason for this discrepancy is the well-known deficiency of the local spin-density approximation to describe correctly the exchange splitting and the easy axis of the magnetocrystalline anisotropy energy in Ni.²⁶

The rotational anisotropy may be determined by considering elliptical precession around a given axis. The two eigenvalues of the damping matrix correspond to the minimal and maximal damping rates obtained when varying the major axis about the precession axis, in the limit of a linear orbit. Previous results of damping rates and those for the orientational anisotropy reported in Fig. 2 are calculated for circular precession. For such calculations, elements of the torque matrix, which is the commutator of the spin-lowering operator σ^- with the spin-orbit Hamiltonian in this case, are evaluated. For elliptical precession σ^- is replaced by an appropriate combination of σ^x and σ^y .

Previous calculations⁸ of the intraband terms according to the breathing Fermi-surface model indicate that the greatest rotational anisotropy occurs for the $\langle 011 \rangle$ orientation of $\mathbf{e}(t)$ in bcc Fe and fcc Ni and near an orientation of $\mathbf{e}(t)$ corresponding to the real-space $(1, 0, 1)/\sqrt{2}$ direction for hcp Co. [We use a coordinate system for which $(0, 0, 1)$ is along the c axis and $(1, 0, 0)$ points toward a nearest-neighbor atom.] Designating these crystallographic axes as the respective \hat{z} directions, we choose $[0\bar{1}1]$ as the \hat{x} direction and $[100]$ as the \hat{y} direction for the calculations on Fe and Ni, and $(-1, 0, 1)/\sqrt{2}$ and $(0, 1, 0)$ as the \hat{x} and \hat{y} real-space directions, respectively, for the Co calculations. By symmetry, these are the principal axes of the damping matrix as found earlier.⁸ Results for the effective damping rate about the \hat{z} direction

for precession with circular (σ^-), elliptical [$(\sqrt{3}\sigma^x - i\sigma^y)/\sqrt{2}$ and $(\sigma^x - i\sqrt{3}\sigma^y)/\sqrt{2}$], and linear ($\sqrt{2}\sigma^x$ and $\sqrt{2}\sigma^y$) orbits are presented in Fig. 3. The effective damping for elliptical precession is an average over the two principal values as determined by the ellipticity of the precession, which can readily be determined from the linearized Gilbert equation with a damping matrix. The damping for the linear precession directly gives the principal values of the damping matrix. We find that the rotational anisotropy of the intraband terms of the torque-correlation model reproduces the previous breathing Fermi-surface results⁸ and are independent of electron scattering rate (temperature). Results of the interband part of the torque-correlation model show rotational anisotropy at low scattering rates but that this anisotropy gradually diminishes with increasing scattering rate (temperature). At scattering rates expected in typical samples at room temperature, damping is dominated by the interband contribution and Fig. 3 suggests that the damping is rotationally isotropic. This trend occurs in each of the three metals and was observed for all other orientations of the magnetization that were tested (not shown).

IV. CONCLUSIONS

We have shown that the conductivitylike contribution to magnetization damping is both orientationally and rotationally anisotropic for all scattering rates τ^{-1} whereas both anisotropies for the resistivitylike contribution decrease with increasing τ^{-1} . The anisotropy of the resistivitylike contribution decreases as the thermal energy becomes comparable to the spin-orbit energy. Therefore, any system will exhibit an isotropic damping at sufficiently high scattering rates. For Ni (for which both the conductivitylike and the resistivitylike contribution could be resolved experimentally²¹) an orientational anisotropy of the linewidth of ferromagnetic resonance FMR has been observed for low temperatures, giving a hint to anisotropic damping, whereas other materials did not show a clear indication for an anisotropic intrinsic FMR linewidth (see Ref. 11 and references therein). We suspect that the orientational anisotropy of α_{eff} would be more prominent in systems with stronger spin-orbit coupling, such as some magnetic semiconductors or materials with perpendicular magnetocrystalline anisotropy.

*faehnle@mf.mpg.de

¹M. Kläui and C. A. F. Vaz, in *Handbook of Magnetism and Advanced Magnetic Materials*, edited by H. Kronmüller and S. Parkin (Wiley, New York, 2007), Vol. 2, p. 879; L. Thomas and S. Parkin, in *Handbook of Magnetism and Advanced Magnetic Materials*, edited by H. Kronmüller and S. Parkin (Wiley, New York, 2007), Vol. 2, p. 942.

²B. Van Waeyenberge, A. Puzic, H. Stoll, K. W. Chou, T. Tylliszczak, R. Hertel, M. Fähnle, H. Brückl, K. Rott, G. Reiss, I. Neudecker, D. Weiss, C. H. Back, and G. Schütz, *Nature (London)* **444**, 461 (2006); M. Curcic, B. Van Waeyenberge, A. Vansteenkiste, M. Weigand, V. Sackmann, H. Stoll, M. Fähnle, T. Tylliszczak, G. Woltersdorf, C. H. Back, and G. Schütz, *Phys. Rev. Lett.* **101**, 197204 (2008); S. Bohlens, B. Krüger, A. Dreuss, M. Bolte, G. Meier, and D. Pfannkuche, *Appl. Phys. Lett.* **93**, 142508 (2008).

³T. L. Gilbert, Ph.D. thesis, Illinois Institute of Technology, 1956.

⁴V. L. Safonov and H. N. Bertram, *Phys. Rev. B* **71**, 224402 (2005).

⁵K. Capelle and B. L. Gyorffy, *Europhys. Lett.* **61**, 354 (2003).

⁶T. L. Gilbert, *IEEE Trans. Magn.* **40**, 3443 (2004).

⁷J. Kuneš and V. Kamberský, *Phys. Rev. B* **65**, 212411 (2002); **68**, 019901(E) (2003).

⁸D. Steiauf and M. Fähnle, *Phys. Rev. B* **72**, 064450 (2005); M. Fähnle, D. Steiauf, and J. Seib, *J. Phys. D* **41**, 164014 (2008); D. Steiauf, J. Seib, and M. Fähnle, *Phys. Rev. B* **78**, 020410(R) (2008); J. Seib, D. Steiauf, and M. Fähnle, *ibid.* **79**, 064419 (2009).

⁹A. Brataas, Y. Tserkovnyak, and G. E. W. Bauer, *Phys. Rev. Lett.* **101**, 037207 (2008).

¹⁰S. Zhang and Steven S.-L. Zhang, *Phys. Rev. Lett.* **102**, 086601

(2009).

¹¹J. Seib, D. Steiauf, and M. Fähnle, *Phys. Rev. B* **79**, 092418 (2009).

¹²C. Vittoria, S. D. Yoon, and A. Widom, *Phys. Rev. B* **81**, 014412 (2010).

¹³B. Heinrich, *Ultrathin Magnetic Structures III* (Springer, New York, 2005).

¹⁴V. Korenman and R. E. Prange, *Phys. Rev. B* **6**, 2769 (1972).

¹⁵V. Kamberský, *Czech. J. Phys., Sect. B* **26**, 1366 (1976).

¹⁶I. Garate and A. MacDonald, *Phys. Rev. B* **79**, 064403 (2009); **79**, 064404 (2009).

¹⁷V. Kamberský, *Can. J. Phys.* **48**, 2906 (1970).

¹⁸K. Gilmore, Y. U. Idzerda, and M. D. Stiles, *J. Appl. Phys.* **103**, 07D303 (2008).

¹⁹K. Gilmore, Y. U. Idzerda, and M. D. Stiles, *Phys. Rev. Lett.* **99**, 027204 (2007).

²⁰V. Kamberský, *Phys. Rev. B* **76**, 134416 (2007).

²¹B. Heinrich, D. J. Meredith, and J. F. Cochrane, *J. Appl. Phys.* **50**, 7726 (1979).

²²B. Heinrich, D. Fraitová, and V. Kamberský, *Phys. Status Solidi* **23**, 501 (1967).

²³M. Fähnle and D. Steiauf, in *Handbook of Magnetism and Advanced Magnetic Materials*, edited by H. Kronmüller and S. Parkin (Wiley, New York, 2007), Vol. 1, p. 282.

²⁴M. D. Stiles, S. V. Halilov, R. A. Hyman, and A. Zangwill, *Phys. Rev. B* **64**, 104430 (2001).

²⁵J. M. Rudd, K. Myrtle, J. F. Cochrane, and B. Heinrich, *J. Appl. Phys.* **57**, 3693 (1985).

²⁶S. Y. Savrasov, A. Toropova, M. I. Katsnelson, A. I. Lichtenstein, V. Antropov, and G. Kotliar, *Z. Kristallogr.* **220**, 473 (2005).